PNAS

Supplementary Information for

Hydrophilic Reentrant SLIPS Enabled Flow Separation for Rapid Water Harvesting

Zongqi Guo, Dylan Boylan, Li Shan, and Xianming Dai*

Department of Mechanical Engineering, University of Texas at Dallas, Richardson, 75080, USA

*Corresponding author: Xianming Dai.

Email: Dai@utdallas.edu

This PDF file includes:

Supplementary text
Figures S1 to S24
Tables S1
Legends for Movies S1 to S9
SI References

Other supplementary materials for this manuscript include the following:

Movies S1 to S9

Supplementary Information Text

Section S1. Sample fabrication and characterization of reentrant channels

We used solid fraction (Φ), surface roughness (R), and channel cross-section area (A) to name the reentrant channel and regular channel (Fig. S2). The solid fraction is calculated as the pitch of the channel to the projecting area:

$$\phi = \frac{P \cdot \Delta L}{(P + W_g) \cdot \Delta L} = \frac{P}{P + W_g} \quad \text{(S1)}$$

where P is the pitch width of the channel top, ΔL is the unit length of the channel, and W_g is the gap between channel top. The surface roughness is calculated as the total surface area with projecting area:

$$R = \frac{S \cdot \Delta L}{(P + W_g) \cdot \Delta L} = \frac{S}{P + W_g} \quad \text{(S2)}$$

For reentrant channel, $S = 2H+P+2(W-W_g)+W_g$. For regular channel, $S = 2H+P+W$. W is the channel width and H is the channel height. Then, the cross-section area A is calculated as:

$$A = W \cdot H \quad \text{(S3)}$$

Section S2. Droplet movement on a flow-separation surface

To achieve flow separation, the first step is to remove droplets condensed on the top of the reentrant structure. Fig. S4 shows the details of the separation process on the top of the reentrant structure. When water vapor nucleates on the top of the reentrant structure, tiny droplets form with a diameter from 1 to 10 μm. Droplets prefer to form on the edge on the top of the reentrant structure due to the edge effect (1, 2). Once droplets condense on the surface, droplets move towards each other and coalesce due to the coarsening effect. Droplet sizes increase mainly by coarsening effect (Fig. S4B). When the meniscus of those droplets connects with the channel edge, droplets are move towards and absorbed by the channel due to coarsening effect. The surface tension force of the oil meniscus is the driving force to move the droplets into the channel (3). When the droplets are removed from the surface, the top of the reentrant structure can condense more water vapor.

In this case, we can separate the vapor from the droplet on the top of the surface. Once the vapor is condensed to form a droplet, the droplets will be removed into the channel. No droplets are shedding along with the gravity above the reentrant structure. The droplet diameter on the reentrant structure top is much smaller than the shedding diameter (D_{max}), which could be calculated by the retention force equation:

$$\rho g V = \gamma(cos\theta_{\mathrm{R}} - cos\theta_{\mathrm{A}}) \cdot D_{\max} \tag{S4}$$

$$V = \frac{\pi(1 - cos\theta)^2(2 + cos\theta)(\bar{D})^3}{24sin^3\theta} \tag{S5}$$

where θ_R is the receding angle, θ_A is the advancing angle, γ is the surface tension of the droplet, ρ is the density of the water droplet, g is the gravitational acceleration, and V is the volume of the droplet. Thus, the top of the reentrant structure will always be fresh to water vapor for nucleation without droplets larger than 50 μm, which is the width of the top of the reentrant structure. The collected droplets inside the channel will be transferred to the bottom of the surface and form droplets with a diameter larger than the shedding diameter (i.e., > 1000 μm). However, on hydrophilic flat SLIPS with coarsening droplets, the surface is always covered by large droplets. Water vapor condenses among water droplets, the surface has a limited area for nucleation. Meanwhile, the droplet transfer to the bottom is mainly relied on shedding droplets. Thus, the condensed water droplets block the water vapor nucleation on the surface.

Coalescence and merging of the liquids from the top of the reentrant surfaces to the channels require the presence of a liquid column inside the channel, which forms in the first place due to the direct vapor condensation inside the channel at the beginning of the condensation (Fig. S5). Due to the hydrophilic nature and concave meniscus inside the microchannel, capillary condensation takes place and rapidly forms liquid columns.

Once the liquid column forms inside the reentrant channel, it enables the droplet removal from the top of the reentrant channel. This is due to the pressure difference between the droplet and liquid column (Fig. S6). When a droplet is condensed on the top of reentrant SLIPS, an oil meniscus forms around the droplet to minimize the surface energy. When the oil meniscus contacts the liquid

column during droplet growth, the oil meniscus acts as a pressure bridge between the droplet and the liquid column.

Pressure difference between droplet and liquid column drives the droplet movement (4). The droplet has a higher pressure as $P_d = P_0 + \Delta P_d = P_0 + 4\gamma\cos\theta/d$, where P_0 is the atmospheric pressure, ΔP_d is the Laplace pressure due to the curvature of droplets, γ is the surface tension force, θ is contact angle, and d is the droplet base diameter (50 μm). The liquid column has a pressure as $P_l = P_0 - \Delta P_l = P_0 - \gamma(1/R_{em} + 1/L)$, where R_{em} is the radius of the liquid column at the emergence interface, and L is the length of the liquid column. Thus, the pressure difference between the droplet and liquid column is $\Delta P = P_d - P_l = \Delta P_d + \Delta P_l \approx 29 + 26 = 55$ *kPa*, which is the driving force to move the droplets from the top to the reentrant channel. Here, the droplet size is 50 μm, the length and width of the liquid column is 200 μm and 25 μm, respectively. Then, we compared the driving force with the pinning force of the droplet. With a contact angle hysteresis of 4°, the pinning force is calculated as: $F_p = 2\gamma(cos\theta_e - cos\theta_{adv}) \cdot D \approx 4.5 \times 10^{-7}\ N$. The driving force acted on the droplet is $F_d = \Delta P \cdot A \approx 6.8 \times 10^{-5}\ N$, which is two orders higher than the pinning force. Thus, droplets can move towards liquid column inside the channel. The flat surface cannot separate water vapor from condensed droplets, which leads to a high coverage ratio (Fig. S7-S9). As a result, the removal frequency of the flat surface is lower than the flow-separation surface due to the limited nucleation area on the surface (Fig. S9).

Section S3. Droplet movement on different surface chemistries

The dimension of the surfaces is 1 × 3 cm (width by length). On hydrophilic non-slippery reentrant, a liquid film forms over the entire surface. Thus, there is no droplet formed at the bottom of the surface due to the high pinning force of the channel. However, droplets are collected at the bottom of the surfaces through the channel or top of the surface on the reentrant SLIPS due to the slippery property. We further analyzed the water harvesting performance by measuring droplet size distribution and coverage ratio on three surfaces (Fig. S14). The hydrophilic reentrant SLIPS collects more droplets on the surface, which has a large number of both tiny droplets (4.9×10^4 /cm^2) and gigantic droplets (2.5 /cm^2). However, there are no gigantic droplets on hydrophilic and

hydrophobic reentrant SLIPS with fewer tiny droplets. Due to the rapid droplet removal of flow separation, the hydrophilic reentrant SLIPS maintains the lowest coverage ratio of 17%. The partial separation can also reduce the coverage ratio to 47%, but the coverage ratio increases to 58% without separation on the hydrophobic reentrant SLIPS. The flow separation can be only achieved by a hydrophilic slippery interface with coarsening effect.

Section S4. Design of flow separation

The flow separation is achieved on both hydrophilic slippery reentrant structure and regular channel, but the lubrication and structure size significantly influence the flow separation performance. For a fair comparison of water harvesting, we fixed the channel area for regular channel and reentrant structure in this study. If it's not specified, the cross-section area is fixed as 2500 μm^2 and the height is varied for a fair comparison. We also fixed the undercut of the reentrant structure as 12.5 ± 3 μm (i.e., $(W\text{-}W_g)/2$).

We found that only hydrophilic reentrant SLIPS can lock the liquid inside the channel and prevent droplets from emerging out of the channel. To further demonstrate the necessity of the reentrant structure, we did the energy analysis for the emergence and elongation of the liquid column considering the pinning forces generated by the sidewalls. The pinning force at the corner of the reentrant overhang is higher than the regular channel, which is related to the three-phase contact line movement across the discontinuous geometry (vertical side wall to horizontal overhang) (5-7). Kim's group reported that the discontinuous geometry provided a larger pinning force than the vertical side wall only (5). During condensation in this work, the liquid column inside the channel is in an equilibrium state shown as state 0 (Fig. S17A). The liquid column is pinned underneath the reentrant overhang with a contact angle of $\theta'_e = 64^o$. θ'_e is the equilibrium contact angle between the liquid column and the oil meniscus at the corner. When the volume of the liquid column increases, the contact line moves horizontally underneath the reentrant undercut to state 1. To emerge out of the reentrant SLIPS, the contact line firstly moves horizontally underneath the overhang, then moves vertically on the side wall of the overhang. The contact angle between the liquid column and the sidewall should reach an advancing angle of $\theta_{adv} = 66^o$. Thus, the contact angle hysteresis is $\theta_{adv} - \theta_e = 66^o$ (Fig. S17A), which is due to the discontinuous geometry. θ_e is

the equilibrium contact angle between the liquid column with the side wall of the overhang. In contrast, the regular channel SLIPS has no overhang or discontinuous geometry on the sidewall. Thus, the contact angle hysteresis is $\theta_{adv} - \theta_e = 2^o$, showing less pinning than the reentrant structure (Fig. S17C). Even though the reentrant SLIPS and regular channel SLIPS have the same contact angle hysteresis due to the same lubrication, the discontinuous geometry changes the direction of the contact line movement and increases the pinning force on reentrant SLIPS (5). When the contact angle of the liquid column increases from the equilibrium contact angle (θ_e) to the advancing angle (θ_{adv}), the liquid column will emerge out of the channel and spread on the top of the surface (Fig. S17). Thus, we calculated the energy of pinning force along the emergence direction as:

$$E_p = 2\gamma(cos\theta_e - cos\theta_{adv}) \cdot L \cdot dH \quad \text{(S6)}$$

where γ is the surface tension of the liquid column, L is the length of the liquid column, and dH is the increased height of the liquid column. Similarly, the liquid column inside a regular channel will advance only along the sidewall of the channel, which has a smaller pinning force than the reentrant structure (Fig. S17C and S17D). Based on the TPCL advancing, for hydrophilic reentrant SLIPS, $\theta_e = 0^o$ at position 2 before TPCL advancing, while $\theta_e = 64^o$ for the regular channel. The θ_{adv} is the same for both hydrophilic reentrant SLIPS and regular channels. For the emergence of the liquid column, the energy of Laplace pressure (driven force of emergence) is (Fig. S17):

$$E_{em} = \Delta P_{em} \cdot A_{em} \cdot dH \quad \text{(S7)}$$

where ΔP_{em} is the Laplace pressure at the interface of emergence, and A_{em} is the top surface of the liquid column perpendicular to emergence direction. By applying the parameters into equation S7, the energy of emergence is:

$$E_{em} = \Delta P_{em} \cdot A_{em} \cdot dH = \gamma\left(\frac{1}{R_{em}} + \frac{1}{R_L}\right) \cdot (L \cdot W_g) \cdot dH$$

$$= \gamma\left(\frac{1}{W_g/2cos\theta_{adv}} + \frac{1}{L/2cos\theta_{adv}}\right) \cdot (L \cdot W_g) \cdot dH \quad \text{(S8)}$$

where R_{em} is the radius of liquid column at emergence interface and R_L is the radius of the liquid column length. Then, we calculated the elongation energy as (Fig. S17):

$$E_{\mathrm{el}} = \Delta P_{\mathrm{el}} \cdot A_{\mathrm{el}} \cdot dL$$

$$= \gamma\left(\frac{1}{R_{\mathrm{W}}} + \frac{1}{R_{\mathrm{H}}}\right) \cdot (H \cdot W) \cdot dL$$

$$= \gamma\left(\frac{1}{W/2cos\theta_{\mathrm{adv}}} + \frac{1}{H/2cos\theta_{\mathrm{adv}}}\right) \cdot (H \cdot W) \cdot dL \quad \text{(S9)}$$

By applying different *L* and *H*, we calculated the energy ratio between emergence energy with pinning force energy and elongation energy (Fig. S19). When the liquid column shows the potential of emergence (i.e., $E_{el}/E_{em} < 1$), only the reentrant structure can lock the liquid column inside the channel as a higher energy barrier generated by pinning force ($E_{p}/E_{em} > 1$).

The channel height is also an important parameter to lock the liquid inside the channels (Fig. S22). The liquid column height is the same as the channel height that determines the $E_{el} \sim F_{el}A_{el}(H)$, where F_{el} is the elongation force. A_{el} is the surface area of the liquid column and is the function of channel height *H*. If the elongation energy is larger than the emergence energy (i.e., $E_{el}/E_{em} > 1$), the droplet will elongate inside the channel instead of emerging out of the channel. The channel height has limited effects on preventing droplet emergence. For a fixed length of the liquid column (i.e., 100 μm), an increased channel height will increase the energy ratio between elongation and emergence E_{el}/E_{em} (Fig. S22).

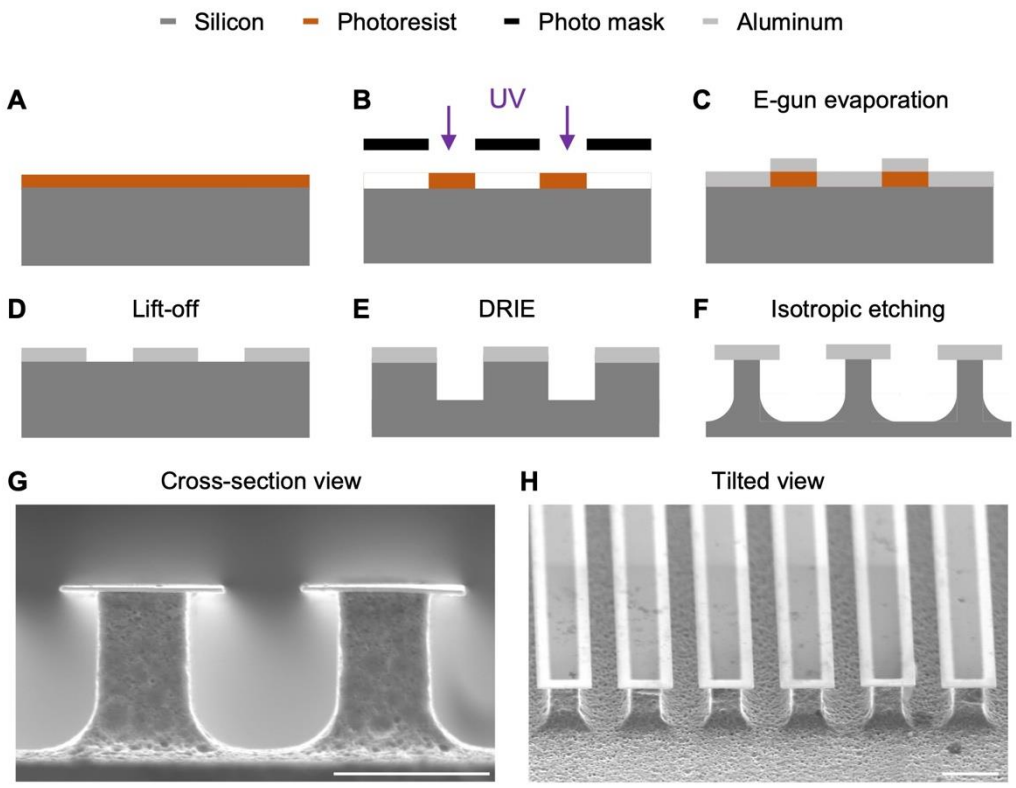

Fig. S1. Fabrication process of reentrant channels. (A) A cleaned silicon wafer is spin-coated with a negative photoresist. **(B)** After photolithography and development, a channel pattern is left on the silicon wafer. **(C)** Aluminum is deposited on a patterned silicon wafer by an e-gun depositor. **(D)** After lift-off, a metal pattern is left on the silicon wafer. **(E)** Patterned silicon wafer is etched by deep reactive ion etching (DRIE) to fabricate regular microchannels. **(F)** To get the reentrant channels, isotropic etching is applied to generate under-cut below aluminum. **(G)** SEM image of reentrant channels from a cross-section view. **(H)** SEM image of reentrant channels from a tilted view. The scale bar is 50 μm for all.

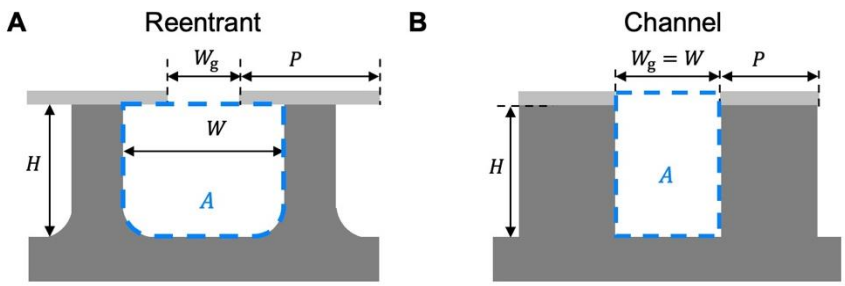

Fig. S2. Parameters of (**A**) reentrant channel, and (**B**) regular channel.

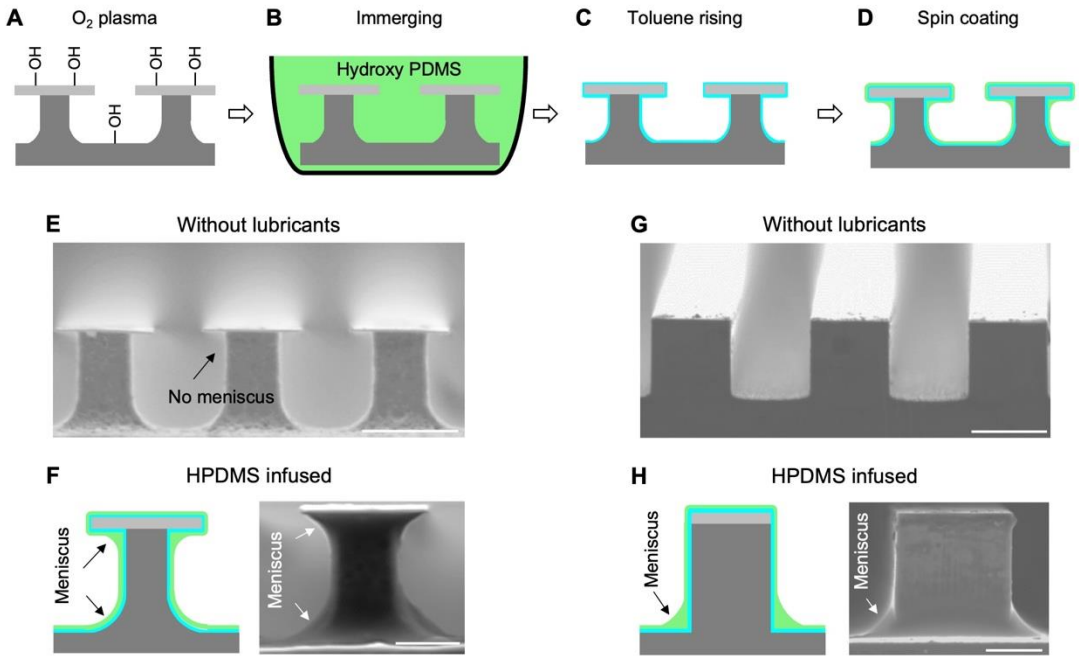

Fig. S3. One-step fabrication process of hydrophilic reentrant SLIPS (slippery liquid infused surface). (**A**) Reentrant channels are treated with oxygen plasma. -OH group is generated on the surface by oxygen plasma. (**B**) Plasma-treated sample is immersed into hydroxy PDMS to form a HQLS coating. (**C**) Extra hydroxy PDMS on HQLS-coated reentrant channels is cleaned by toluene rising. (**D**) Different oil lubricants (e.g., HPDMS or silicone oil) is spin-coated on HQLS-coated reentrant channels. SEM of reentrant structure without lubricant (**E**) and infused with HPDMS (**F**). SEM of regular channel without lubricant (**G**) and infused with HPDMS (**H**). The scale bar is 50 μm for all.

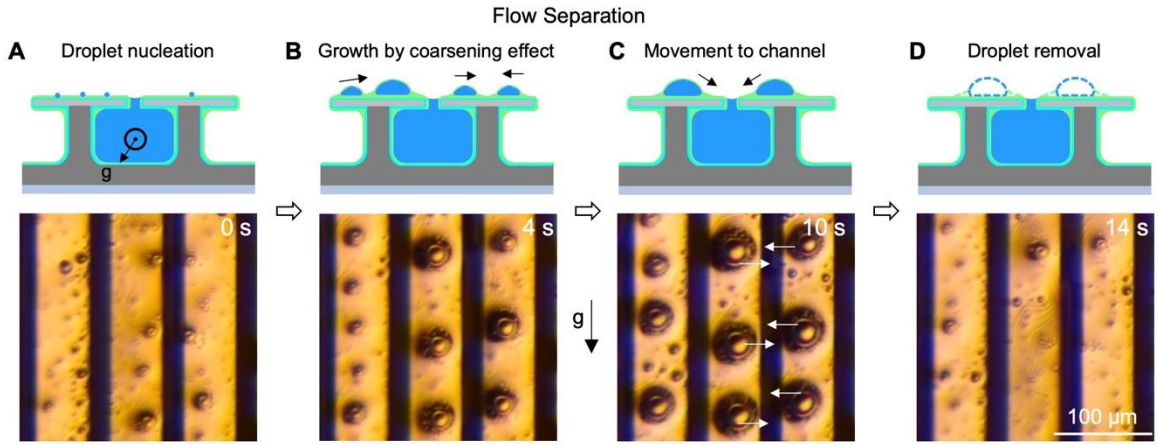

Fig. S4. Flow separation mode on hydrophilic reentrant SLIPS. (**A**) Droplet nucleation on the top of the reentrant SLIPS. (**B**) Nucleated droplets grow by coarsening effect. (**C**) Droplets move towards the channel as shown by white arrows. (**D**) Droplets are removed from the surface. The scale bar is 100 µm for all.

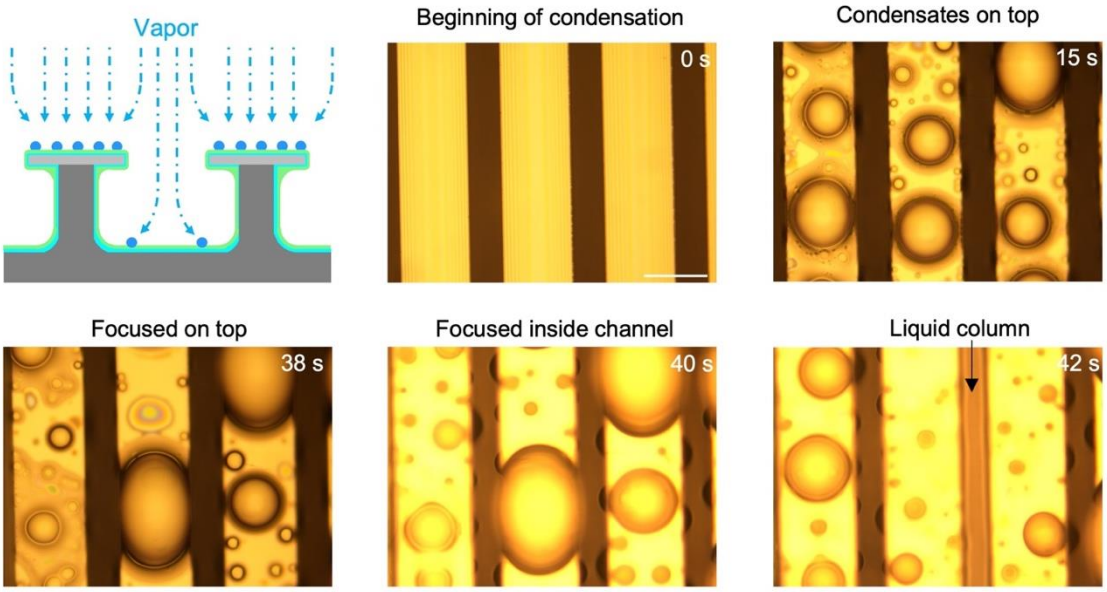

Fig. S5. Vapor condensation on hydrophilic reentrant SLIPS at the beginning stage. Channels condensed fewer droplets than top. The scale bar is 100 μm.

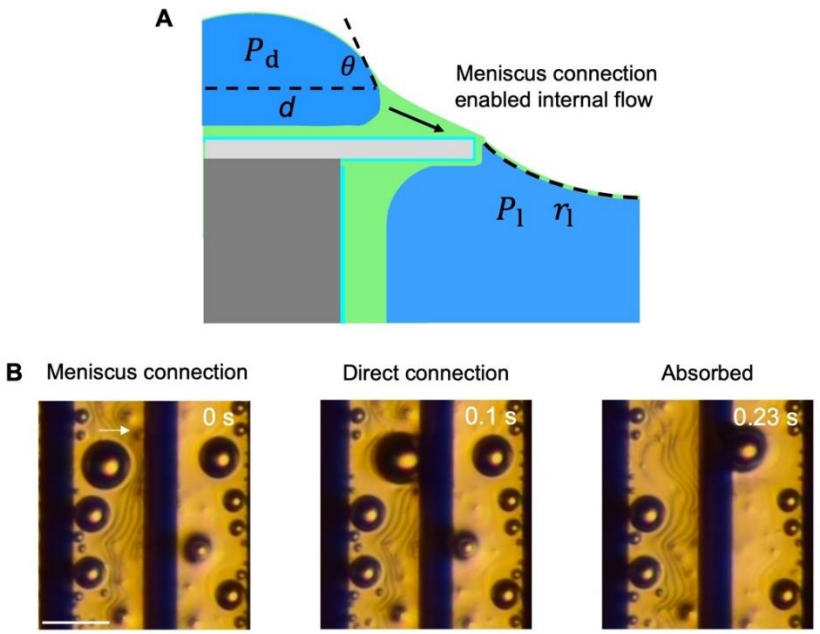

Fig. S6. Droplet movement on reentrant top. (**A**) Schematic of pressure in a droplet and liquid column. (**B**) Microscope image of droplet movement on Reentrant top. The scale bar is 50 μm.

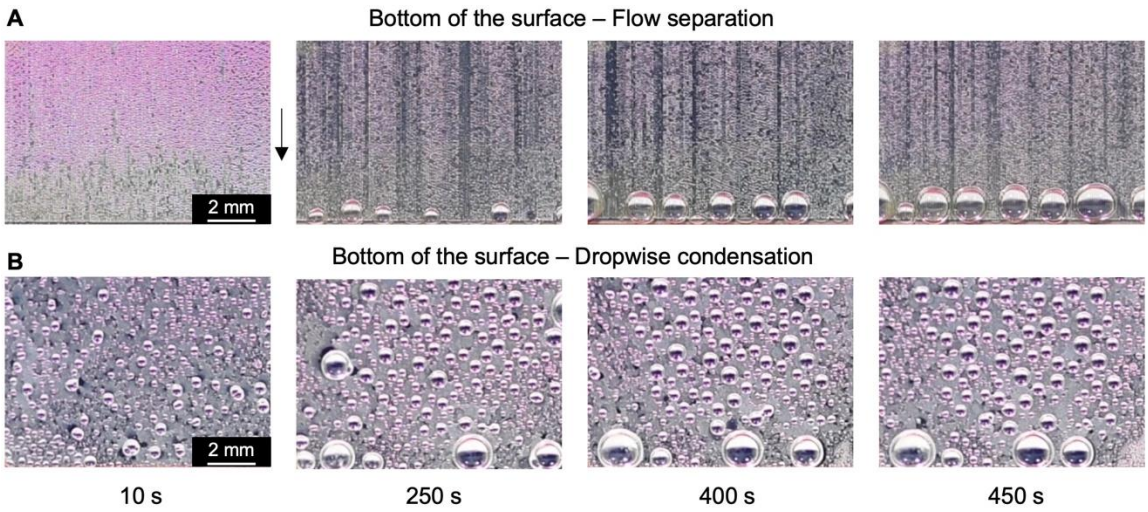

Fig. S7. Droplet size distribution at the bottom of (**A**) hydrophilic reentrant SLIPS with flow separation and (**B**) flat SLPS with coarsening droplets.

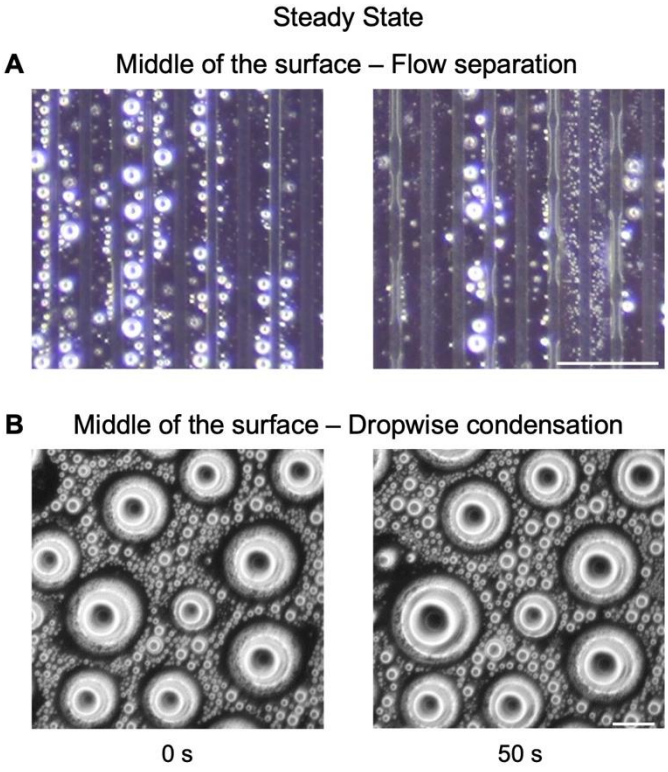

Fig. S8. Droplet size distribution in the middle of the surface. (**A**) Droplet size distribution in the middle of the surface from flow separation. (**B**) Droplet size distribution in the middle of the surface from coarsening droplet. The scale bar is 200 μm.

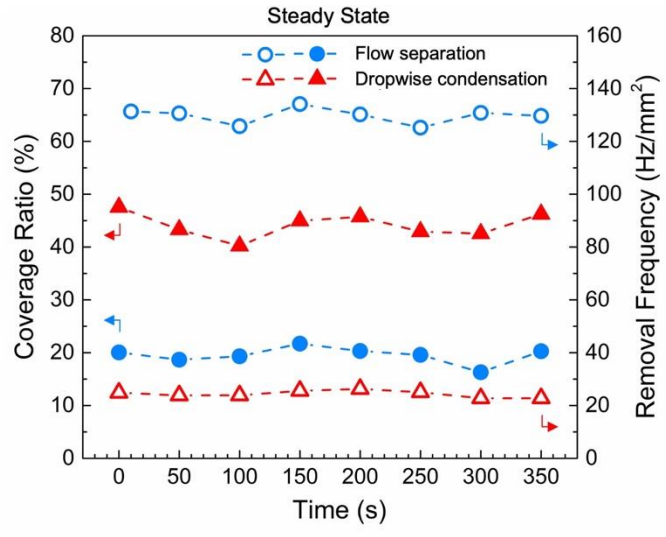

Fig. S9. Water coverage ratio φ and droplet removal frequency f of flow separation and dropwise condensation with time. The blue triangles (hollow or solid) present the hydrophilic reentrant SLIPS with flow separation. The red triangles (hollow or solid) present the HPDMS-infused flat SLIPS with coarsening droplets.

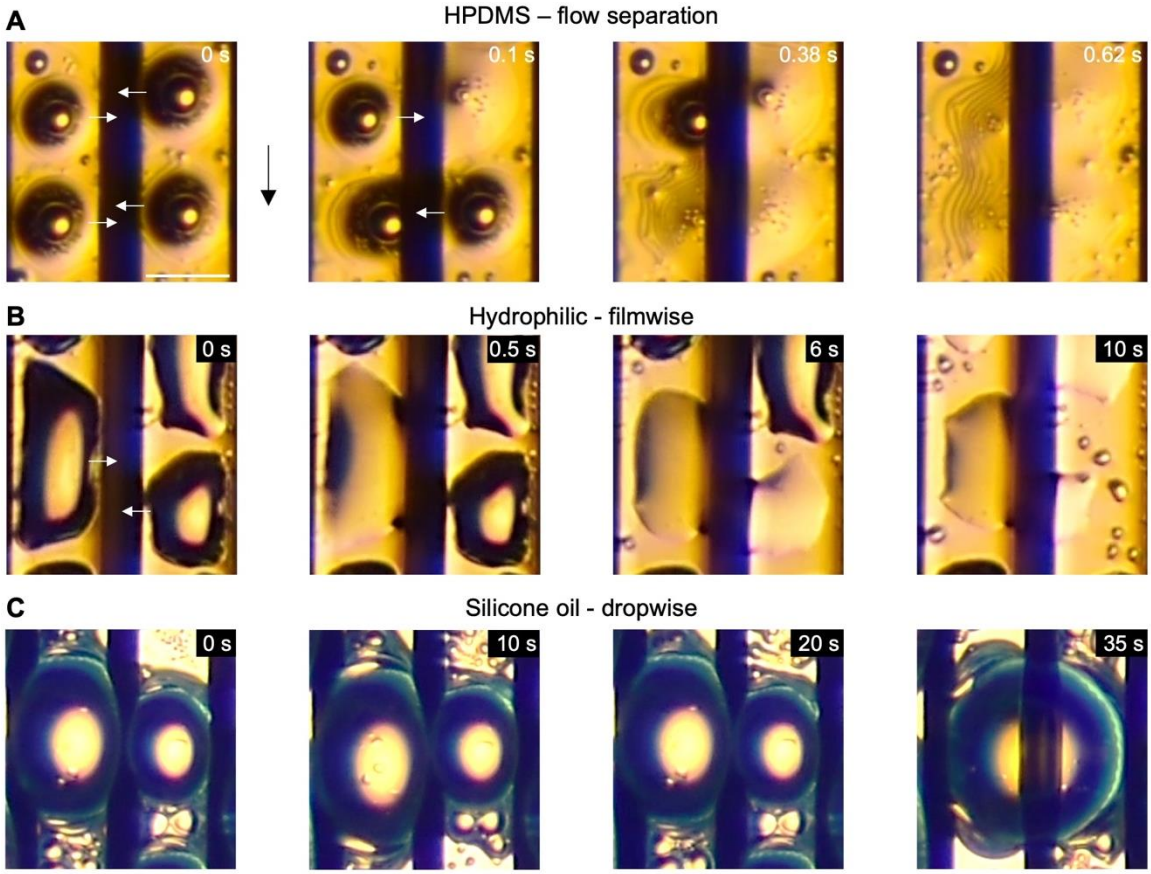

Fig. S10. Droplet movement on surfaces with different surface chemistries. (**A)** Droplet movement on a hydrophilic reentrant SLIPS during water harvesting tests. Droplets move to the channel due to meniscus-mediated coarsening effect. The white arrow shows the droplet movement towards channel. (**B)** Droplet movement on a hydrophilic bare reentrant. Droplets are removed into the channel by direct contact. The white arrow shows the droplet is absorbed by channel. (**C)** Droplet movement on a hydrophobic reentrant SLIPS. The scale bar is 50 μm for all. The arrow shows the direction of gravity.

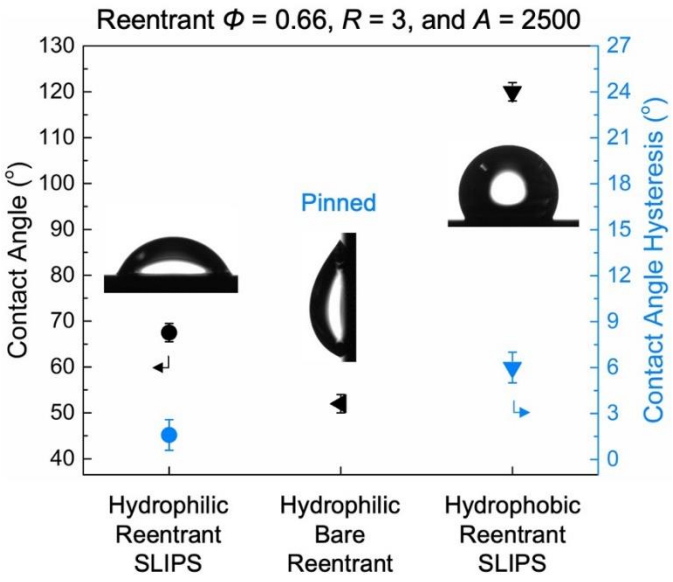

Fig. S11. Contact angle and contact angle hysteresis on surfaces with different surface chemistries. Droplet is pinned on hydrophilic reentrant structure.

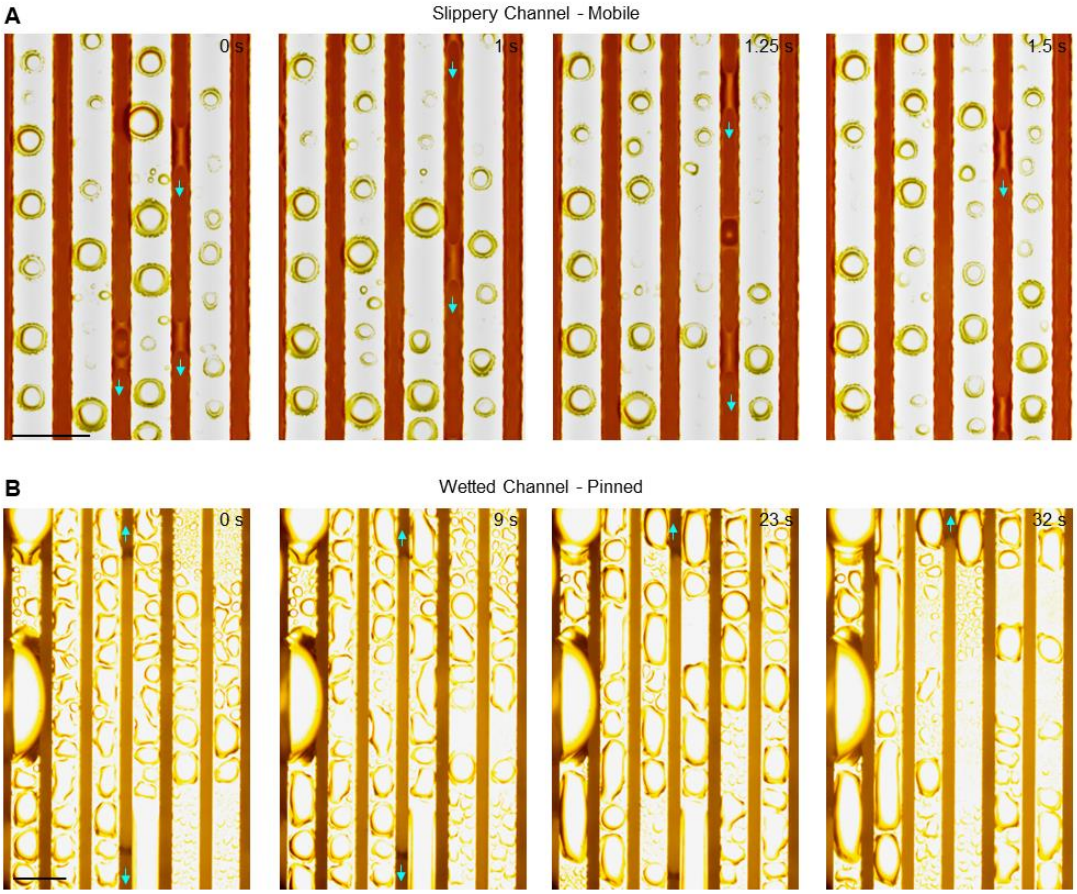

Fig. S12. Droplet movement inside the channel. (**A**) Liquid shedding inside a slippery channel of hydrophilic reentrant SLIPS. The arrow shows the liquid column shedding inside channel. (**B**) Liquid wetting inside hydrophilic channel. Liquid column has no movement. The arrow shows the water wetting inside channel. The scale bar is 50 μm.

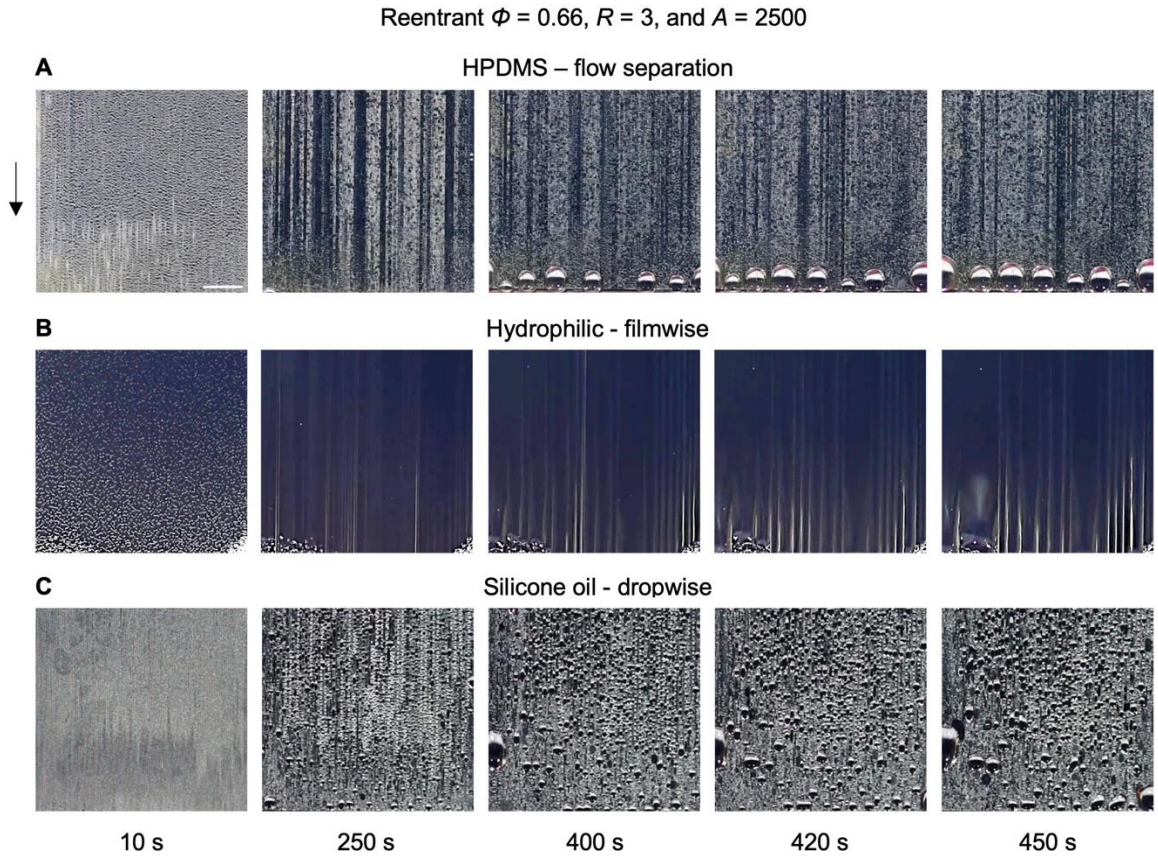

Fig. S13. Droplet size evolution during condensation process of (**A**) Flow separation on hydrophilic reentrant SLIPS, (**B**) Partial flow separation on hydrophilic bare reentrant structure, and (**C**) Dropwise condensation on hydrophobic reentrant SLIPS. The scale bar is 2.5 mm for all. The arrow shows the direction of gravity.

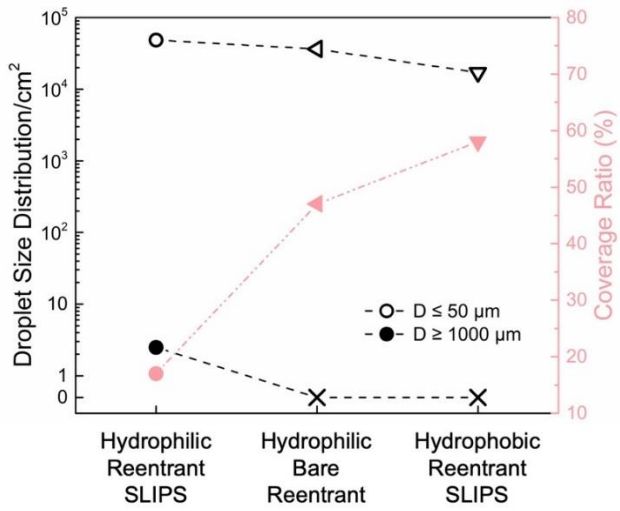

Fig. S14. Droplet size distribution and coverage ratio vary with the surfaces. The data were collected at 400 s after the first nucleation on the surface.

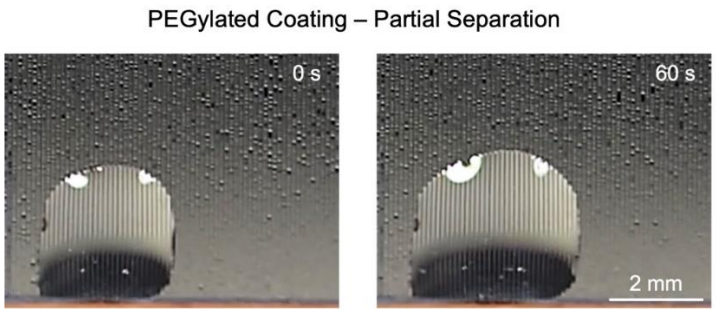

Fig. S15. Condensation on PEGylated microchannels. Macro view of droplets collected at the bottom of the surface showing partial flow separation. The scale bar is 2 mm.

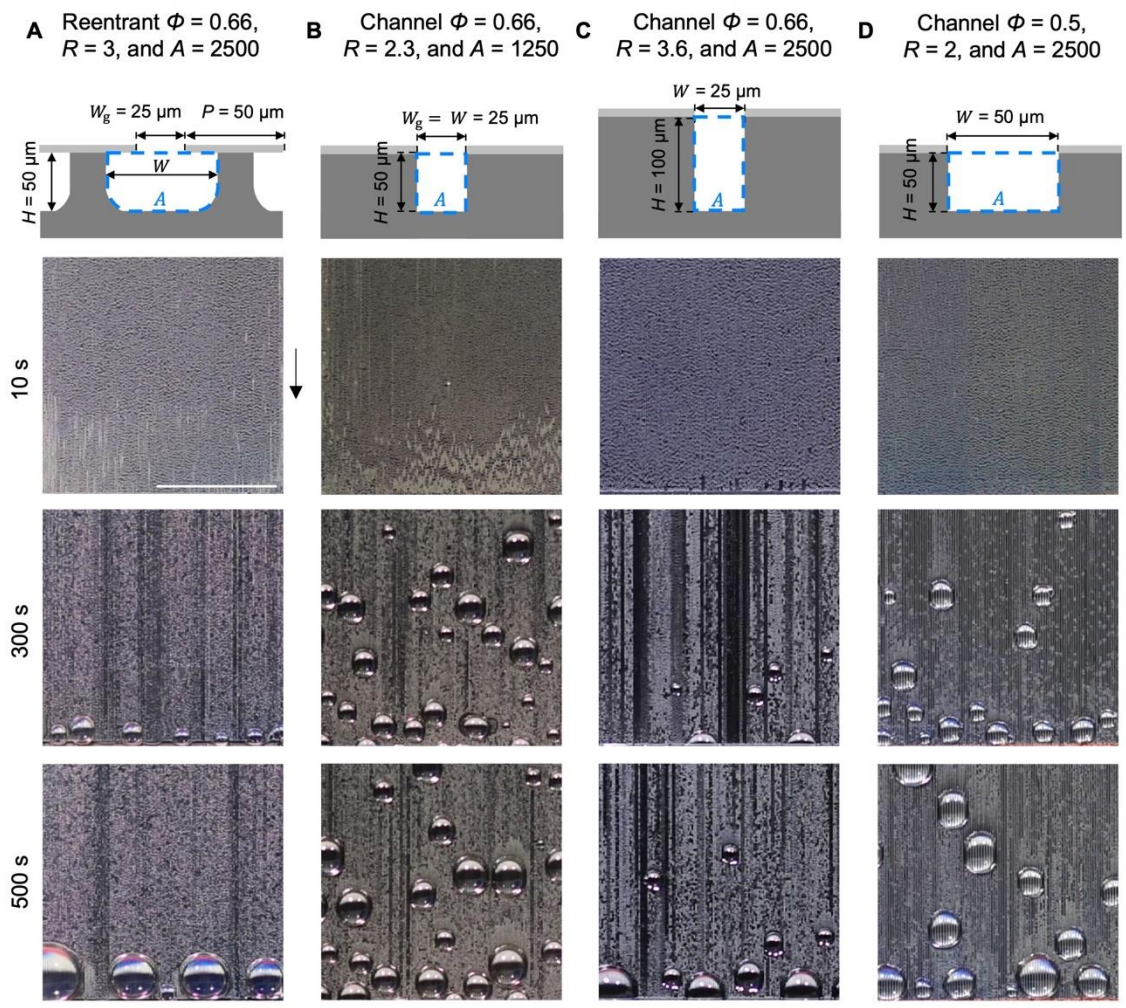

Fig. S16. Condensation on hydrophilic reentrant SLIPS and hydrophilic slippery channels with different solid fraction. Water harvesting performance on hydrophilic reentrant SLIPS of (**A**) Reentrant Φ = 0.66 and R = 3. Water harvesting performance on hydrophilic slippery channel of (**B**) Channel Φ = 0.66 and R = 2.3, (**C**) Channel Φ = 0.66 and R = 3.6, and (**D**) Channel Φ = 0.5 and R = 2. The scale bar is 5 mm. The arrow shows the direction of gravity.

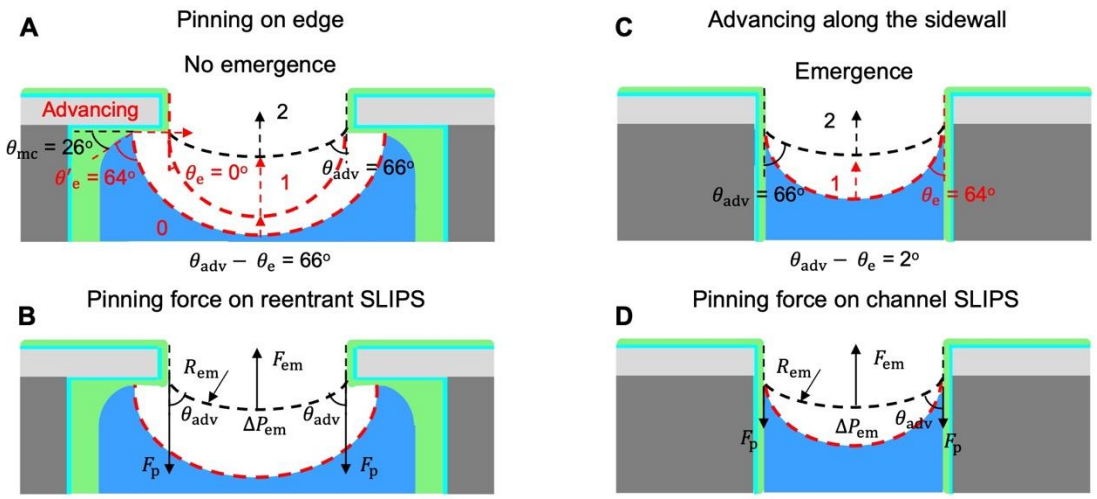

Fig. S17. Pinning and driven force analysis of droplet emergence. (**A**) Schematic of three-phase contact line movement on hydrophilic reentrant SLIPS. (**B**) Schematic of pinning force and emergence force on reentrant structure. (**C**) Schematic of three-phase contact line movement on regular channel. (**D**) Schematic of pinning force and emergence force on regular channel.

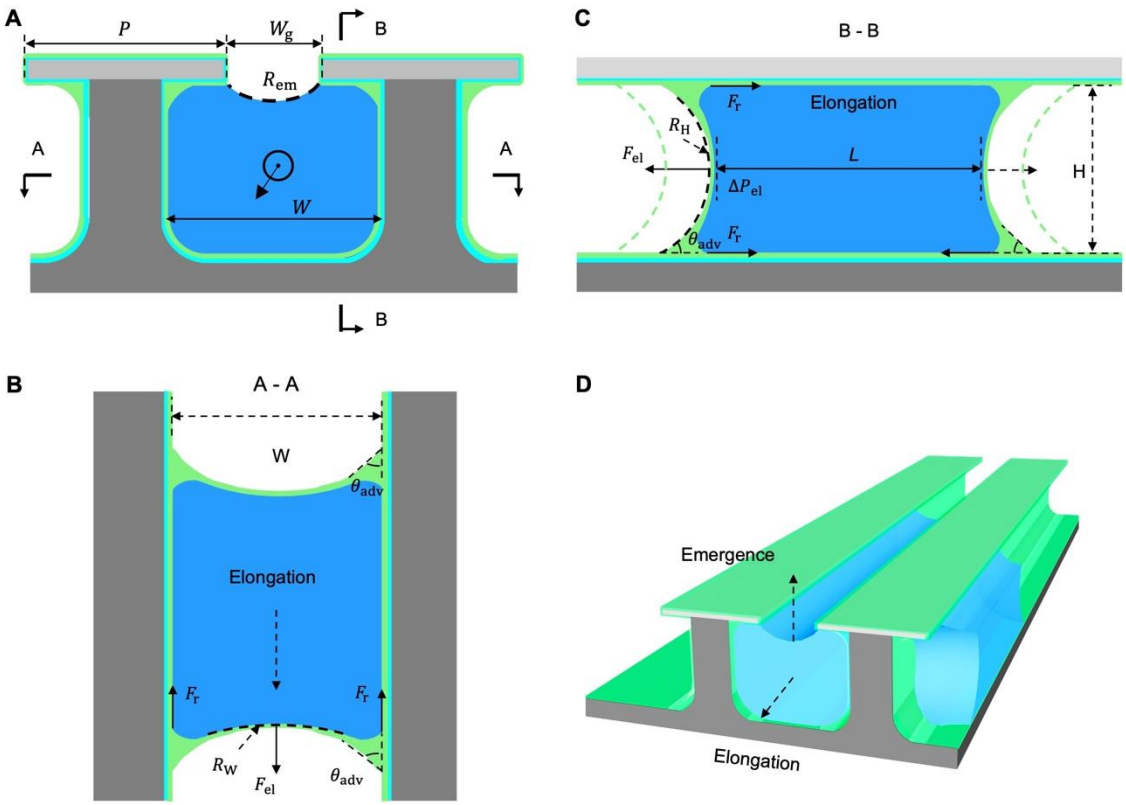

Fig. S18. Elongation force analysis. (**A**) Cross-section of hydrophilic reentrant SLIPS. (**B**) Schematic of A-A section of reentrant SLIPS. (**C**) Schematic of B-B section of reentrant SLIPS. (**D**) Schematic of overall droplet movement.

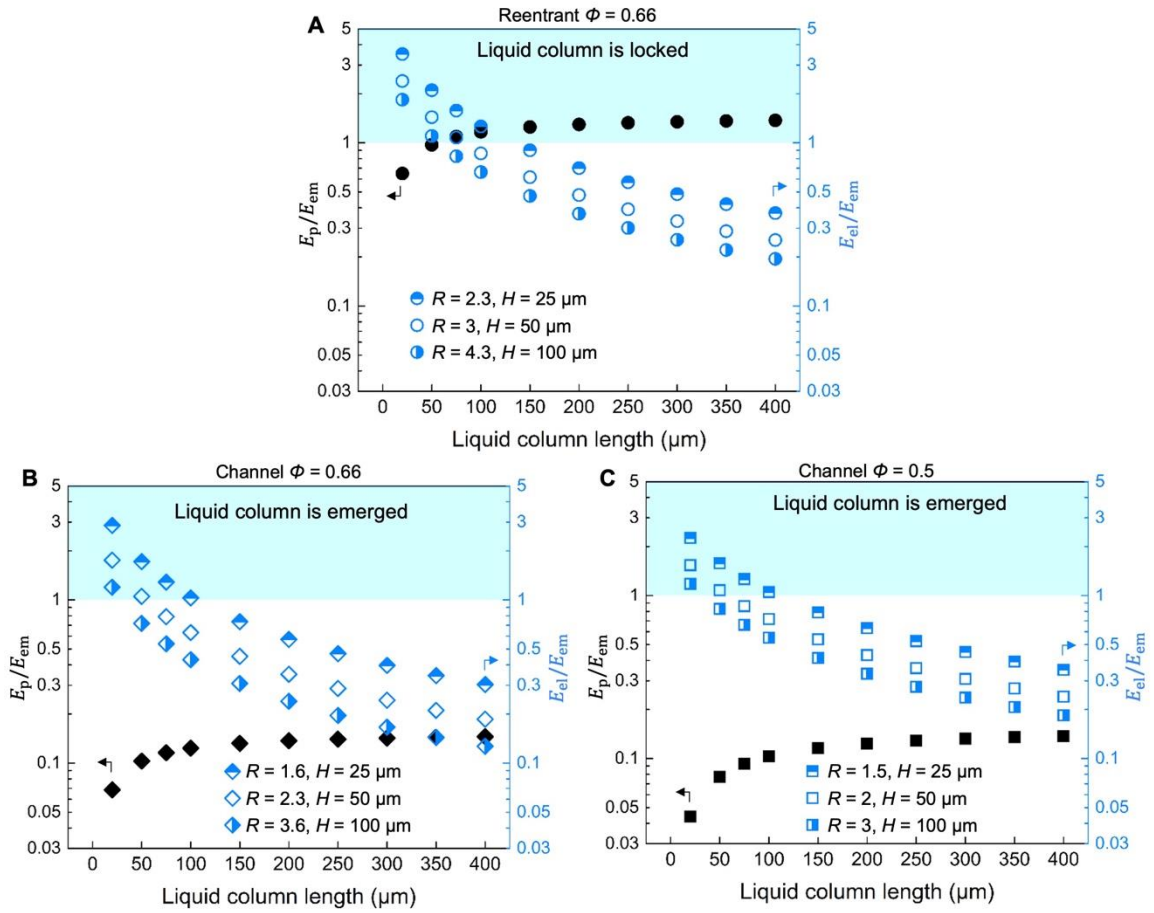

Fig. S19. Energy analysis of emergence energy (E_{em}) with elongation movement (E_{el}) and emergence pinning energy (E_p) for (**A**) hydrophilic reentrant SLIPS Φ = 0.66 with different surface roughness, (**B**) hydrophilic regular channel Φ = 0.66 with different surface roughness, and (**C**) hydrophilic regular channel Φ = 0.5 with different surface roughness.

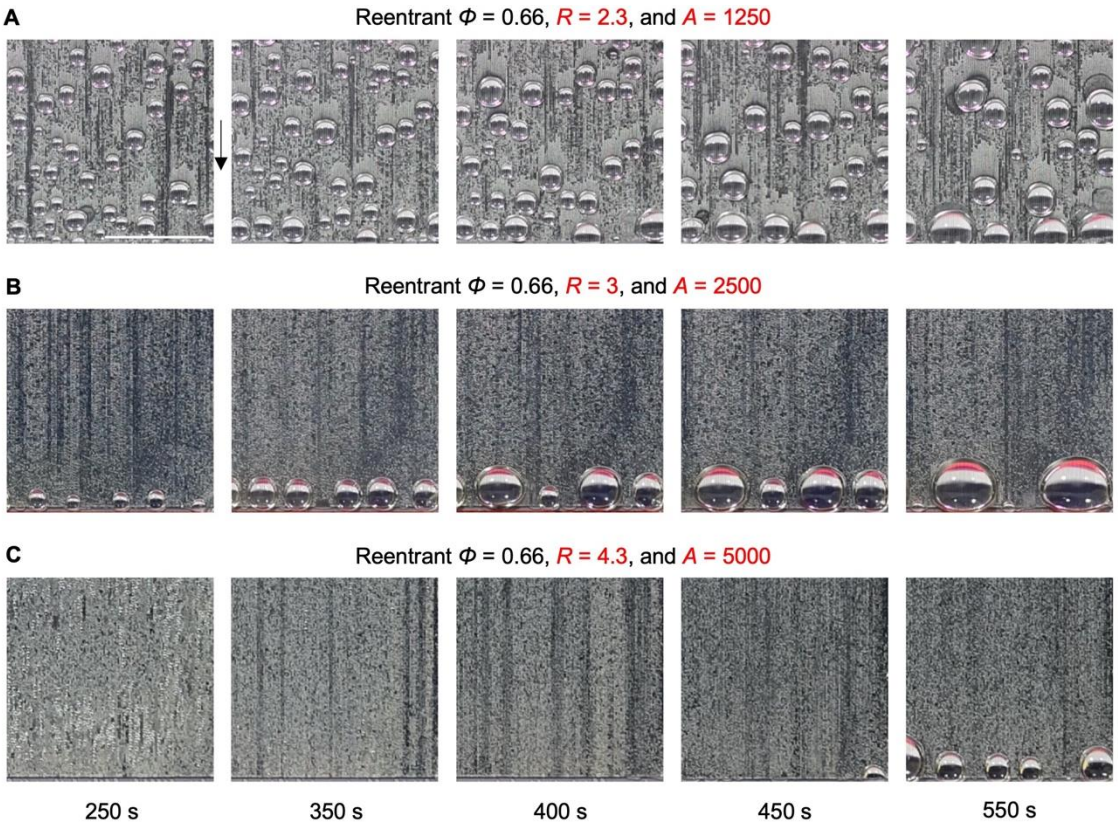

Fig. S20. Condensation on hydrophilic reentrant SLIPS with a roughness *R* of (**A**) 2.3, (**B**) 3, and (**C**) 4.3. The scale bar is 5 mm. The arrow shows the direction of gravity.

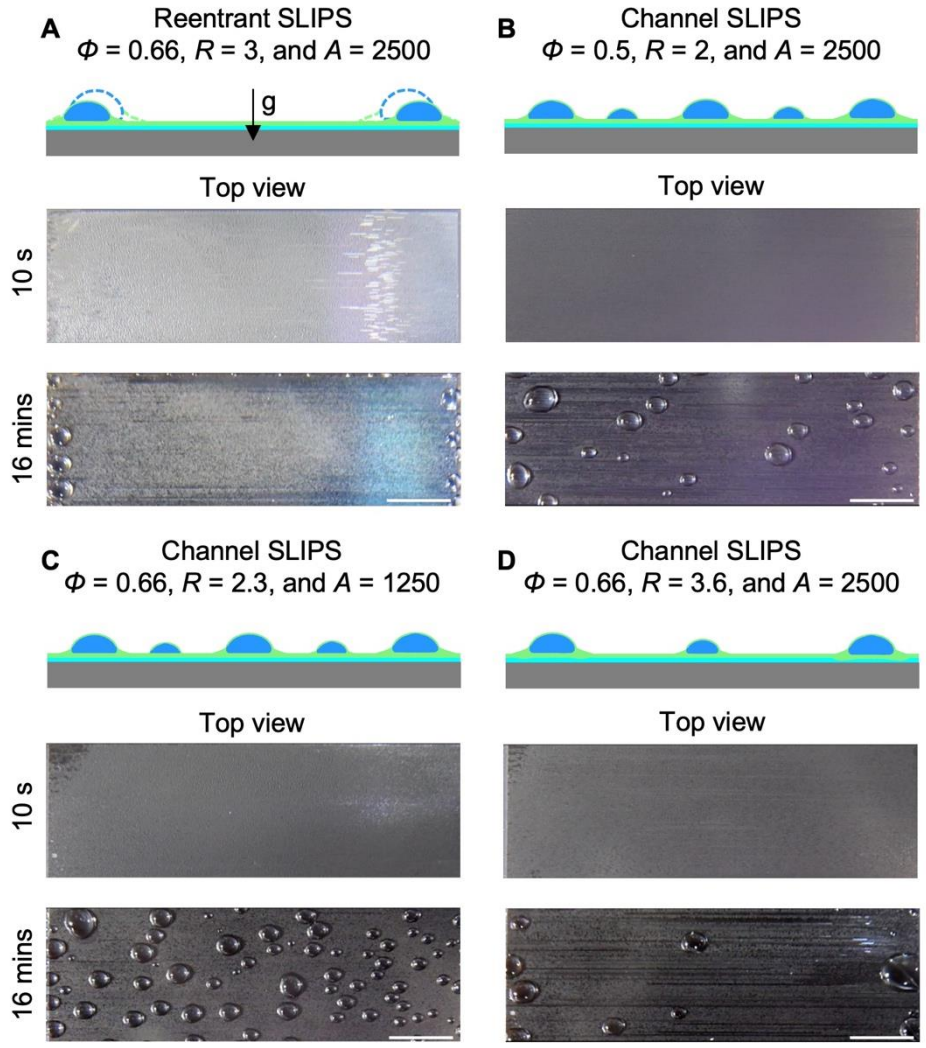

Fig. S21. Horizontal setup - condensation on hydrophilic reentrant SLIPS and hydrophilic slippery channels with different solid fractions. Water harvesting performance on hydrophilic reentrant SLIPS of (**A**) Reentrant $\Phi = 0.66$ and $R = 3$. Water harvesting performance on hydrophilic slippery channel of (**B**) Channel $\Phi = 0.5$ $R = 2$, (**C**) Channel $\Phi = 0.66$ and $R = 2.3$, and (**D**) Channel $\Phi = 0.66$ and $R = 3.6$. The scale bar is 5 mm. The arrow shows the direction of gravity.

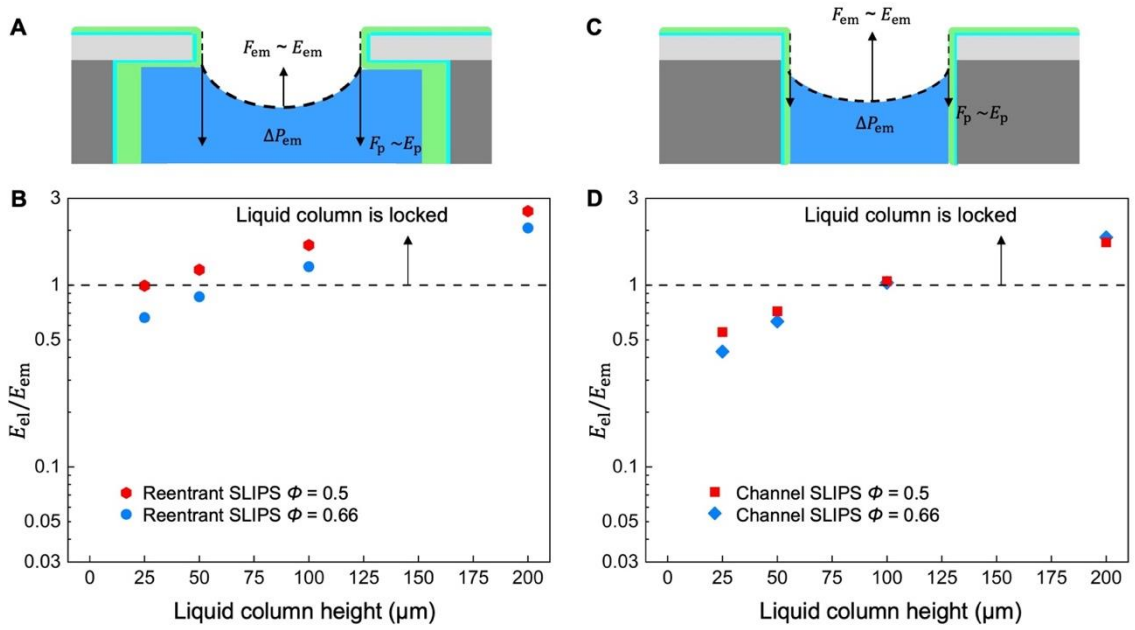

Fig. S22. Elongation energy compared with emergence energy based on different liquid column heights. (**A**) Schematic of forces on hydrophilic reentrant SLIPS. The elongation energy $E_{el} \sim F_{el}A_{el}(H)$. (**B**) Energy ratio on hydrophilic reentrant SLIPS with different liquid column heights. (**C**) Schematic of forces on hydrophilic channel SLIPS. (**D**) Energy ratio on hydrophilic channel SLIPS with different liquid column heights. The liquid column length is 100 μm.

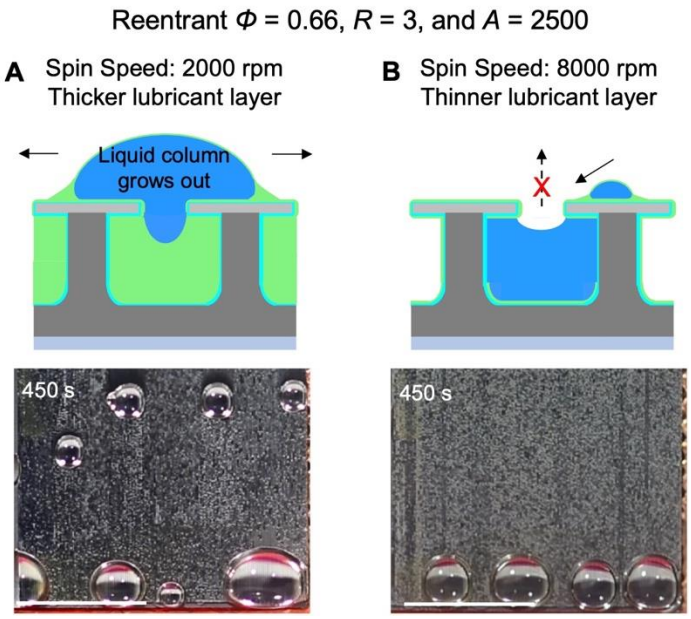

Fig. S23. Condensation on hydrophilic reentrant SLIPS with a spin speed of (**A**) 2000 rpm with droplet emergence due to low pinning force, and (**B**) 8000 rpm. The scale bar is 5 mm.

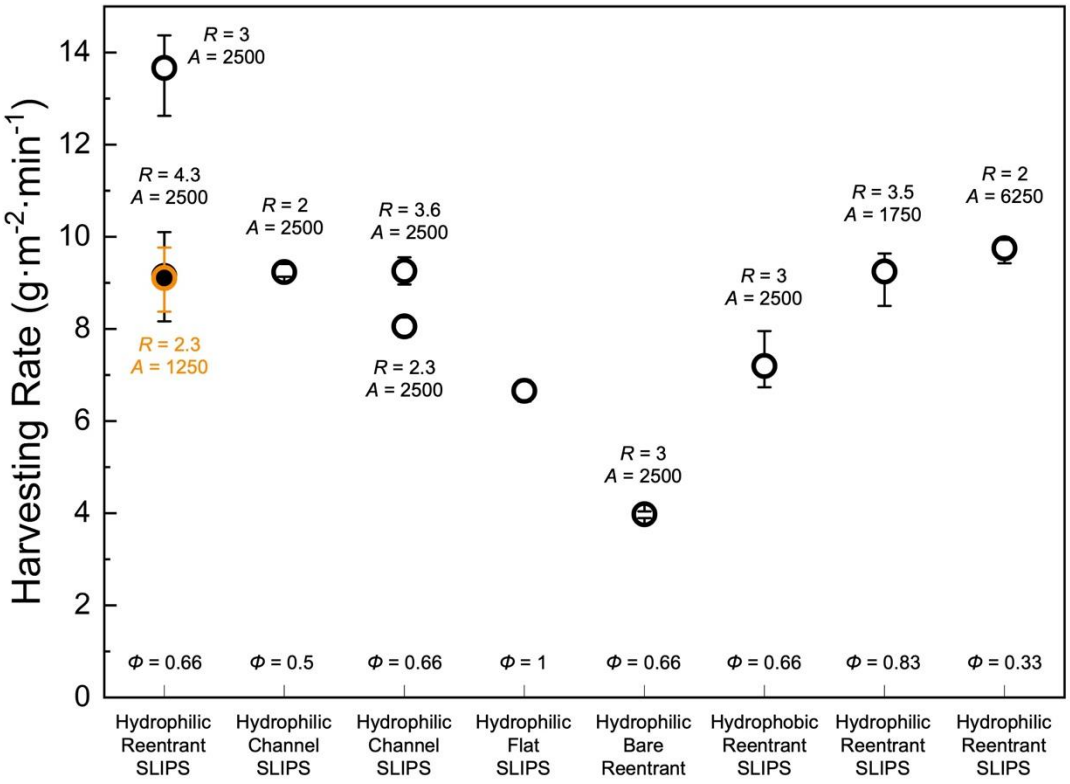

Fig. S24. Water harvesting rates on all the tested surfaces.

Table S1. Contact angle and contact angle hysteresis on reentrant channel and regular channel with different coatings.

	SLIPS – HPDMS		HQLS		Without coating	
	Contact Angle (± 1°)	Contact Angle Hysteresis (°)	Contact Angle (± 1°)	Contact Angle Hysteresis (°)	Contact Angle (± 1°)	Contact Angle Hysteresis (°)
Flat	69.6	1.1± 0.5	102.1	25.2 ± 3	64.5	Pinned
Channel Φ = 0.66	63.2	6.1 ± 1	105.6	18.4 ± 1	13.5	
Channel Φ = 0.5	61.8	2.7 ± 0.5	129.4	10.1 ± 1	26.8	
Reetrant Φ = 0.66	67.5	2.0 ± 0.5	105.4	16.5 ± 1	52.6	

Note: The droplet volume is 5 µL. Contact angle and contact angle hysteresis on reentrant structure and regular channel are measured from the side view of the channel. Droplet is in Wenzel state on HPDMS and without coating (1, 2).

Movie S1. Flow separation *versus* dropwise condensation. The lubricant is hydroxy PDMS with a spin speed of 4000 rpm. The white arrow shows the direction of gravity. Videos are sped up by 2X.

Left: Flow separation on a hydrophilic reentrant SLIPS (Reentrant Φ = 0.66 and R = 3). Once droplets are nucleated on the lubricant, they are removed by coarsening effect towards the reentrant channels. The surface has no droplets with diameters larger than 50 μm. The scale bar is 100 μm.

Right: Dropwise condensation with coarsening droplet on a hydrophilic flat SLIPS. Once small droplets are nucleated on the lubricant, they are removed by coarsening effect towards a large one. Large droplets are pinned on the surface until they reach the shedding diameter. The scale bar is 200 μm.

Movie S2. Droplet growth at the bottom surfaces in a steady state. The lubricant is hydroxy PDMS with a spin speed of 4000 rpm. The white arrow shows the direction of gravity. The scale bar is 2 mm. Videos are sped up by 15X.

Left: Flow separation on a hydrophilic reentrant SLIPS (Φ = 0.66 and R = 3). The surface has no visible droplets. All droplets are transported into the channel and collected at the bottom of the surface.

Right: Dropwise condensation with shedding droplets on a hydrophilic flat SLIPS. The surface is covered by lots of large droplets. Droplet growth at the bottom is dependent on droplet shedding.

Movie S3. Microscope view of droplet growth at the bottom surfaces. The lubricant is hydroxy PDMS with a spin speed of 4000 rpm. The white arrow shows the direction of gravity. The scale bar is 500 μm. Videos are sped up by 15X.

Left: Flow separation on a hydrophilic reentrant SLIPS (Φ = 0.66 and R = 3). The surface does not have droplets with diameters above 50 μm. All big droplets move into the reentrant channels and transport to the bottom of the surface.

Right: Dropwise condensation with shedding droplets on a hydrophilic flat SLIPS. The surface is covered by lots of visible droplets. Droplet growth at the bottom is dependent on droplet shedding.

Movie S4. Microscope view of droplet size distribution in the middle of the surface. The lubricant is hydroxy PDMS with a spin speed of 4000 rpm. The white arrow shows the direction of gravity. Videos are in real-time.

Left: Flow separation on a hydrophilic reentrant SLIPS (Φ = 0.66 and R = 3). The surface does not have droplets with diameters above 50 μm. All big droplets move into the reentrant channels. The scale bar is 250 μm.

Right: Dropwise condensation with shedding droplets on a hydrophilic flat SLIPS with the coarsening droplet. It has a larger coverage ratio. The scale bar is 500 μm.

Movie S5. Mechanism of flow separation – hydrophilic reentrant SLIPS. The substrates are reentrant channels $\Phi = 0.66$ and $R = 3$ with different surface coatings. The white arrow shows the direction of gravity. The scale bar is 100 μm. Videos are sped up by 2X.
Left: Flow separation on hydrophilic reentrant SLIPS infused with hydroxy PDMS. The spin speed is 4000 rpm. All big droplets move into the reentrant channels.
Middle: Partial separation on hydrophilic bare reentrant channels. The surface has no coating. Droplets move into the reentrant channels but leave residue due to the high pinning forces.
Right: Dropwise condensation on hydrophobic reentrant SLIPS infused with silicone oil. The spin speed is 4000 rpm. Droplets coalesce on the surface and lead to non-wetting.

Movie S6. Mechanism of flow separation – slippery channel. The substrates are reentrant channels $\Phi = 0.66$ and $R = 3$ with different surface coatings. The white arrow shows the direction of gravity. The scale bar is 100 μm. Videos are in real-time.
Left: Flow separation on hydrophilic reentrant SLIPS infused with hydroxy PDMS. The spin speed is 4000 rpm. All big droplets move into the reentrant channels. Liquid columns transport inside to the end of each reentrant channel.
Right: Partial flow separation on hydrophilic bare reentrant channels. The surface has no coating. Droplets move into the reentrant channels but leave residues. The liquid columns wet the reentrant channels due to the high pinning forces.

Movie S7. Macro view of water harvesting on different coatings. The substrates are reentrant channels $\Phi = 0.66$ and $R = 3$ with different surface coatings. The white arrow shows the direction of gravity. The scale bar is 5 mm.
Left: Flow separation on hydrophilic reentrant SLIPS infused with hydroxy PDMS. The spin speed is 4000 rpm. All droplets are collected at the bottom of the surface.
Middle: Partial flow separation on hydrophilic bare reentrant channels. The surface has no coating. Droplets move into the reentrant channels but leave residues due to the high pinning forces. The surface shows a filmwise condensation.
Right: Dropwise condensation on hydrophobic reentrant SLIPS infused with silicone oil. The spin speed is 4000 rpm. Droplets coalesce on the surface but cannot be absorbed by the hydrophobic channel. The surface is covered by large droplets.

Movie S8. Flow separation – droplet growth. The lubricant is hydroxy PDMS with a spin speed of 4000 rpm. The white arrow shows the direction of gravity. The scale bar is 200 μm.

Top left: Hydrophilic reentrant SLIPS (Φ = 0.66 and R = 3) infused with hydroxy PDMS shows no droplet out of the reentrant channels.
Others: Three hydrophilic channel SLIPS infused with hydroxy PDMS. The spin speed is 4000 rpm. All three surfaces show droplets out of the channels.

Movie S9. Flow separation during dew harvesting. Only hydrophilic reentrant SLIPS (Φ = 0.66 and R = 3) shows the flow separation while other surfaces only show partial flow separation with shedding droplets. The out-of-channel droplets reduced the efficiency of dew harvesting as they isolate the surface with vapor. The lubricant is hydroxy PDMS with a spin speed of 4000 rpm. The white arrow shows the direction of gravity. The scale bar is 5 mm.

SI References

1. Y. Zhao *et al.*, Effects of millimetric geometric features on dropwise condensation under different vapor conditions. *Int. J. Heat Mass Transf.* **119**, 931-938 (2018).
2. X. Dai, B. B. Stogin, S. Yang, T.-S. Wong, Slippery wenzel state. *Acs Nano* **9**, 9260-9267 (2015).
3. Z. Guo, L. Zhang, D. Monga, H. A. Stone, X. Dai, Hydrophilic slippery surface enabled coarsening effect for rapid water harvesting. *Cell Rep. Phys. Sci.* **2**, 100387 (2021).
4. C.-W. Lo, Y.-C. Chu, M.-H. Yen, M.-C. Lu, Enhancing Condensation Heat Transfer on Three-Dimensional Hybrid Surfaces. *Joule* **3**, 2806-2823 (2019).
5. T. L. Liu, C.-J. C. Kim, Turning a surface superrepellent even to completely wetting liquids. *Science* **346**, 1096-1100 (2014).
6. A. Tuteja *et al.*, Designing superoleophobic surfaces. *Science* **318**, 1618-1622 (2007).
7. D. Liao, M. He, H. Qiu, High-performance icephobic droplet rebound surface with nanoscale doubly reentrant structure. *Int. J. Heat Mass Transf.* **133**, 341-351 (2019).